EFDA–JET–PR(10)63

F. Imbeaux, J. Citrin, J. Hobirk, G.M.D. Hogeweij, F. Köchl, V.M. Leonov, S. Miyamoto, Y. Nakamura, V. Parail, G. Pereverzev, A. Polevoi, I. Voitsekhovitch, V. Basiuk, R. Budny, T. Casper, J. Fereira, A. Fukuyama, J. Garcia, Y.V. Gribov, N. Hayashi, M. Honda, I.H. Hutchinson, G. Jackson, A.A. Kavin, C. E. Kessel, R.R. Khayrutdinov, C. Labate, X. Litaudon, P.J. Lomas, J. Lönnroth, T. Luce, V.E. Lukash, M. Mattei, D. Mikkelsen, I. Nunes, Y. Peysson, P. Politzer, M. Schneider, G. Sips, G. Tardini, S.M. Wolfe, V.E. Zhogolev, ASDEX Upgrade Team, C-Mod Team, DIII-D Team, JT-60U Team, Tore Supra Team, contributors of the EU-ITM ITER Scenario Modelling group, ITPA “Integrated Operation Scenarios” group members and experts, ITPA “Transport and Confinement” group members and experts and JET EFDA contributors

Current Ramps in Tokamaks: From Present Experiments to ITER Scenarios

Current Ramps in Tokamaks: From Present Experiments to ITER Scenarios

F. Imbeaux[1], J. Citrin[2], J. Hobirk[3], G.M.D. Hogeweij[2], F. Köchl[4], V.M. Leonov[5], S. Miyamoto[6], Y. Nakamura[7], V. Parail[8], G. Pereverzev[3], A. Polevoi[3], I. Voitsekhovitch[8], V. Basiuk[1], R. Budny[10], T. Casper[9], J. Fereira[11], A. Fukuyama[12], J. Garcia[1], Y.V. Gribov[9], N. Hayashi[6], M. Honda[6], I.H. Hutchinson[13], G. Jackson[14], A.A. Kavin[15], C.E. Kessel[10], R.R. Khayrutdinov[5], C. Labate[16], X. Litaudon[1], P.J. Lomas[8], J. Lönnroth[17], T. Luce[14], V.E. Lukash[5], M. Mattei[18], D. Mikkelsen[10], I. Nunes[5], Y. Peysson[1], P. Politzer[10], M. Schneider[1], G. Sips[19], G. Tardini[3], S. M. Wolfe[13], V.E. Zhogolev[12], ASDEX Upgrade Team, C-Mod Team, DIII-D Team, JT-60U Team, Tore Supra Team, contributors of the EU-ITM ITER Scenario Modelling group, ITPA "Integrated Operation Scenarios" group members and experts, ITPA "Transport and Confinement" group members and experts and JET EFDA contributors

JET-EFDA, Culham Science Centre, OX14 3DB, Abingdon, UK

[1]CEA, IRFM, F-13108 Saint Paul Lez Durance, France
[2]FOM Institute for Plasma Physics Rijnhuizen, Association EURATOM-FOM, Nieuwegein, The Netherlands
[3]Max-Planck-Institut für Plasmaphysik, EURATOM-Assoziation, Garching, Germany
[4]Association EURATOM-ÖAW/ATI, Vienna, Austria
[5]RRC "Kurchatov Institute", Moscow, Russia
[6]Japan Atomic Energy Agency, 801-1, Mukouyama, Naka, Ibaraki-ken 311-0193, Japan
[7]Nippon Advanced Technology Co., Ltd. Tokai, Ibaraki 319-1112 Japan
[8]EURATOM-CCFE Fusion Association, Culham Science Centre, OX14 3DB, Abingdon, OXON, UK
[9]ITER Organization, Route de Vinon sur Verdon, F-13115 St Paul lez Durance, France
[10]Princeton Plasma Physics Laboratory, P.O. Box 451, Princeton, NJ USA
[11]Association Euratom-IST, Lisboa, Portugal
[12]Kyoto University, Sakyo-ku, Kyoto, 606-8501 Japan
[13]Plasma Science and Fusion Center, MIT, Cambridge, MA USA
[14]General Atomics, San Diego, USA
[15]NIIEFA, St. Petersburg, Russia
[16]Associazione ENEA/CREATE, DIMET, Università di Reggio Calabria Via Graziella, 89100, Calabria, Italy
[17]Association EURATOM-TEKES, Helsinki University of Technology, Finland
[18]Associazione ENEA/CREATE, DIAM, Seconda Università di Napoli Via Roma 29, 81031, Aversa, Italy
[19]EFDA CSU, JET, Culham Science Centre, OX14 3DB, Abingdon, OXON, UK
** See annex of F. Romanelli et al, "Overview of JET Results", (23rd IAEA Fusion Energy Conference, Daejon, Republic of Korea (2010)).*

Preprint of Paper to be submitted for publication in
Nuclear Fusion

ABSTRACT.
In order to prepare adequate current ramp-up and ramp-down scenarios for ITER, present experiments from various tokamaks have been analysed by means of integrated modelling in view of determining relevant heat transport models for these operation phases. A set of empirical heat transport models for L-mode (namely the Bohm-gyroBohm model and scaling based models with a specific fixed radial shape and energy confinement time factors of $H_{96\text{-}L} = 0.6$ or $H_{IPB98} = 0.4$) has been validated on existing experiments for predicting the *li* dynamics within +/− 0.15 accuracy during current ramp-up and ramp-down phases. Simulations using the Coppi-Tang or GLF23 models (applied up to the LCFS) overestimate or underestimate the internal inductance beyond this accuracy (more than +/− 0.2 discrepancy in some cases). The most accurate heat transport models are then applied to projections to ITER current ramp-up, focusing on the baseline inductive scenario (main heating plateau current of $I_p = 15$MA). These projections include a sensitivity study to various assumptions of the simulation. While the heat transport model is at the heart of such simulations (because of the intrinsic dependence of the plasma resistivity on electron temperature, among other parameters), more comprehensive simulations are required to test all operational aspects of the current ramp-up and ramp-down phases of ITER scenarios. Recent examples of such simulations, involving coupled core transport codes, free boundary equilibrium solvers and a Poloidal Field (PF) systems controller are also described, focusing on ITER current ramp-down.

1. INTRODUCTION

The scenario design of a future tokamak device naturally focuses on the main heating phase, where fusion reactions take place. Nevertheless, the conditions to access, and eventually to terminate smoothly, the desired main heating state is also an essential topic. The main heating phase is usually carried out at high plasma current, since in a tokamak high current means high confinement. This current is ramped up from a negligible value just after the plasma breakdown to a plateau value, usually mainly by inductive means. After the main heating phase, the plasma current and energy content must also be ramped down smoothly before stopping the plasma discharge. There are several issues to be addressed during plasma current ramp phases of tokamak operation: MagnetoHydroDynamic (MHD) activity can take place and lead to early plasma termination, depending on the shape of the plasma current density profile. The design of the Poloidal Field (PF) system and plasma shape controller must allow ramping up the plasma current while providing stable plasma equilibrium. In addition, a significant amount of magnetic flux is needed to ramp the plasma up inductively, thus the flux consumption during the current ramp is also a key element in the design of the PF system. Finally, the confinement / MHD properties of the final "main heating" phase depend on the q-profile obtained at the end of the ramp-up and may be optimised by applying additional heating and non-inductive current drive during the current ramp.

Current ramp down in ITER is also quite a challenging part of plasma operation. Apart from the issue of not exceeding the density limit, a burning plasma is usually in H mode before the current

ramp-down and shall return to L-mode before termination. During the H-L transition the plasma quickly loses energy content, which needs to be properly handled by the vertical stability system.
In order to prepare adequate current ramp-up and ramp-down scenarios for ITER, present experiments from various tokamaks (mainly JET, and also ASDEX Upgrade, Tore Supra) have been analysed by means of integrated modelling in view of determining heat transport models relevant for the current ramp-up and ramp-down phases. The results of these studies are presented (section 2.1) and projections to ITER current ramp-up and ramp-down scenarios are done (section 2.2), focusing on the baseline inductive scenario (main heating plateau current of I_p = 15MA).

While the heat transport model is at the heart of such simulations (because of the intrinsic dependence of the plasma resistivity on electron temperature, among other parameters), more comprehensive simulations are required to test all operational aspects of the current ramp-up and ramp-down phases of ITER scenarios. Recent examples of such simulations, involving coupled core transport codes, free boundary equilibrium solvers and a PF systems controller are described in section 3.

2. HEAT TRANSPORT STUDIES FOR CURRENT RAMP-UP

We present here simulations aiming at validating heat transport models on existing experiments, then use the validated models for extrapolation to ITER. The simulations reported in this section are solving the one-dimensional (radial direction) fluid transport equations on poloidal magnetic flux (current diffusion equation) and electron and ion heat transport. The radial coordinate used in this section is the square root of the normalised toroidal flux ρ. The equilibrium is calculated consistently with the results of the transport equations, using fixed boundary solvers. When analysing present experiments, the shape of the Last Closed Flux Surface (LCFS) prescribed in the simulation is determined from magnetic measurements.

2.1 VALIDATING HEAT TRANSPORT MODELS AGAINST PRESENT CURRENT RAMP-UP EXPERIMENTS

A database of 8 discharges, mainly from the JET tokamak, has been selected covering ohmic current ramp-up cases, as well as ramp-up assisted with moderate additional heating (up to a few MW). While JET dominates the dataset, a few experiments from Tore Supra and ASDEX Upgrade have been used as well, in order to test the validity of the models for different machine size and plasma shape, which is quite important in view of extrapolation to ITER. Up to now, this heat transport model validation effort has essentially been conducted by modellers from the ITER Scenario Modelling group of the European Integrated Tokamak Modelling Task Force (see[1] for a presentation of the first results of this group), using the three major European transport codes, namely ASTRA[2], CRONOS [3] and JETTO [4]. This has been the occasion of detailed code benchmarking, quite useful to detect possible mistakes in simulation parameterization and numerical problems, as well as to verify the details of the implementation of the transport models.

The current diffusion and heat transport equations for the electron and ion channels are solved consistently. The boundary condition for solving the electron heat transport equation is prescribed from the measured temperature in the vicinity of the last closed flux surface. In some cases (LHCD or very early phases of the discharges), the measurements close to the plasma edge are of poor quality and the uncertainty on the *Te* (electron temperature) boundary condition to use is large. This uncertainty influences the absolute internal inductance *li* prediction, depending on the transport model used (typically a difference of 0.05 in *li* is obtained when varying the temperature boundary condition from a factor of 3 for the Bohm-gyroBohm model, the scaling-based models are found less sensitive). In most cases, *Ti* (ion temperature) measurements are missing and we use *Ti* = *Te* at the boundary. Table 1 presents a quantitative analysis of these uncertainties for one example in our shot database. The electron density profile is prescribed from measurements (Abel inversion of line-integrated interferometer measurements). Flat Z_{eff} profile is assumed, with a uniform value of Z_{eff} prescribed from Bremsstrahlung measurements. We also prescribe the radiated power profile from Abel inversion of bolometry measurements, when available. Toroidal rotation is not taken into account. As no or moderate NBI power was used plasma rotation is expected to be low and have negligible impact on heat transport. The equilibrium is recalculated using a fixed boundary equilibrium solver, while the dynamics of the plasma boundary are prescribed from pre-existing equilibrium reconstruction constrained by magnetic measurements.

The internal inductance has been chosen as essential parameter / criterion for validation of the heat transport models in the context of current ramp-up and ramp-down phases. Several definitions exist for *li*. In this paper we choose the one known as *li(3): li ((3)* = $\frac{2V\langle B_P^2\rangle}{(m_0 I_P)^2 R_0}$ (where *V* is the plasma volume, I_p the plasma current, R_0 the major radius of the plasma and $\langle\ \rangle$ denotes average over the whole plasma volume : $\langle B_P^2\rangle$ $1/V \int B_P^2\, dV$,). This parameter is important from the operational point of view since i) the range of current profile shapes that can be sustained by the Poloidal Field coils can be characterised by an interval of *li*; ii) *li* is a key parameter for the vertical instability; iii) *li* is also a key parameter for typical Magneto-Hydrodynamical (MHD) activity during the ramp-up.

Being a normalised volume averaged quantity, the internal inductance is strongly weighted by the outer half of the plasma. Therefore details of the current density profile inside mid-radius have a weak impact on the *li* value. The prediction of *li* dynamics depends essentially on the electron temperature profile outside mid-radius. Even if the heat transport model deviates from the *Te* measurements inside mid-radius, or is not accurate on the ion temperature prediction, it may be judged relevant for the prediction of this key operational parameter.

The models tested are the following :

- Scaling-based models, using a fixed radial shape $\chi(\rho,t) = A(t)(1 + 6\,\rho^2 + 80\,\rho^{20})$. This shape is relatively flat throughout the plasma core, then presents a rapid increase of the diffusivity close to the LCFS, reproducing the general trend deduced from interpretative analysis of the our ramp-up experimental dataset. The time-dependent factor A(t) is adjusted at each call of the model in order that the plasma thermal energy content W_{th} follows a known scaling expression, namely: $W_{th} = H\tau_E (P_{loss} - \dot{W}_{th})$. In this expression, $\dot{W}_{th}$ denotes the time derivative of W_{th} and P_{loss} the power lost through the separatrix. Two scaling expressions for the energy confinement time τ_E have been used : the ITER96-L (L-mode) [5] scaling and the IPB98 (H-mode) scaling[6]. The optimal agreement between experiment and simulations (using *li* and flux consumption as criterion) with this model in our current ramp-up dataset is obtained using either $H_{96\text{-}L} = 0.6$ or $H_{IPB98} = 0.4$. Interestingly, the energy confinement time during current ramp-up phases of selected DIII-D and C-MOD discharges (not included in the validation dataset yet) follow approximately the same *H* factors, which strengthens the confidence in this scaling-based approach.

- The empirical Bohm/gyro-Bohm model, in its original L-mode version without magnetic shear dependence [7].
- The Coppi-Tang model [8]
- The GLF23 model [9], applied either up to the LCFS ("GLF23 full rad." on figures) or substituted by a constant diffusion coefficient of 8 m^2/s in the edge region $0.8 < \rho < 1$ ("GLF23 $\rho < 0.8$" on figures), see below for the motivation for this substitution

Figures 1-6 present some typical highlights of this comparison of the models to experimental data, which includes both ohmic and discharges with moderate heating during the current ramp-up. On the JET ohmic Pulse No: 71827 the Bohm/gyro-Bohm and the GLF23 with edge substitution models are most accurate in *Te* and *li* while the scaling-based models tend to slightly overestimate Te in the core (Figs. 1 and 2). However this behaviour is not general. The Coppi-Tang model grossly overestimates the electron temperature and *li*.

For the JET discharge #72823, which features 2 MW of Lower Hybrid Current Drive (LHCD) and 1.5 MW of Neutral Beam Injection (NBI, diagnostic beam) the Bohm/gyro-Bohm and scaling-based models describe the *li* and electron temperature dynamics with the same satisfying accuracy (Figs.3 and 4). In this discharge, LHCD has an important influence of the *li* and Te dynamics in the current ramp-up and must be carefully modelled. The optimal reconstruction of the experimental data here is obtained by a significant ad-hoc broadening the LH power deposition and current drive profiles with respect to the results of the used LHCD solver (DELPHINE Ray-tracing / Fokker-Planck solver within CRONOS) [10][11]. The need for this ad-hoc broadening, which appears frequently when carrying out detailed comparison to experimental data (see e.g. [11]), could be due to LH physics elements missing in this simulation, such as i) taking into account the full launched power spectrum (as a function of the parallel refractive index) instead of a simple two lobes description, ii) taking into account the scattering of LH waves induced by density fluctuations. Using this broadening procedure and depending on the transport model, the target q-profile at the end of the current ramp-up can be reconstructed within 0.5 accuracy with respect to a Motional Stark Effect and magnetic measurements constrained equilibrium reconstruction (Fig.4, right).
Using the first-principle based GLF23 model in the current ramp-up phase is a challenge, in

particular because our figure of merit (the accuracy in predicting the internal inductance) is strongly weighted by what happens in the outer half of the plasma. When applied up to the LCFS, the GLF23 model tends to predict very low level of transport resulting in a sort of pedestal in *Te*, which is not consistent with the experimental data and leads to a strong underestimation of *li* (Figs. 4 and 8). This behaviour seems to be general on our dataset and is a major caveat for the application of GLF23 in the ramp-up phase. In order to correct this problem, the model has been arbitrarily patched in the region $0.8 < \rho < 1$ by prescribing a fixed diffusion coefficient $\chi_e = \chi_i = 8\ m^2/s$. With this patch, GLF23 provides rather accurate *li* and *Te* dynamics on the JET shots, though still has problems reproducing the *Te* profile on Tore Supra.

For the Tore Supra case (Figs.5 and 6) the scaling-based models are the most accurate in terms of electron temperature. As a consequence they are also the most accurate for correlating the time of occurrence of the first sawtooth in experiment and the occurrence of the q = 1 surface in the simulations (see Table 2).

The AUG discharge in our dataset (Figs.7 and 8) is not reproduced as well by the models so far. The reason is most probably that the outer third of this discharge is impurity dominated (unboronised machine) and a careful treatment of the radiated power must be applied in the simulation. The outer part of this plasma is strongly cooled by radiation, so that *Te* is still below 50 eV in the region $0.6 < \rho < 1$ at t = 0.34 s. This region of surprisingly low *Te* for confined tokamak plasmas gradually reduces as the current is ramped-up but still covers $0.8 < \rho < 1$ at t = 0.5s (already half of the flat-top plasma current has been ramped-up). Without a proper treatment of this quite peculiar situation in terms of radiated power, our simulations cannot capture such dynamics and predict higher temperature in the outer half of the plasma, thus delaying the current penetration and underestimating *li*. Eventually, during the current flat-top the scaling-based and Bohm/gyro-Bohm models recover a relatively accurate prediction of the electron temperature profile and of the *li* value within the previous error bar of +/− 0.15.

The main conclusion of this study is that the Bohm/gyro-Bohm and scaling-based models are the most accurate ones for modelling the L-mode current ramp-up phase of at least two different tokamaks, yielding on our dataset (but the AUG radiation dominated discharge) the correct *li* dynamics within +/− 0.15.

2.2 PROJECTIONS TO ITER

Using the most accurate transport models (Bohm/gyro-Bohm and scaling-based), projections to the ITER current ramp-up phase are carried out. The GLF23 model with edge substitution is also used for comparison, though we do not recommend its use for extrapolation to ITER owing to the arbitrariness of the $\chi_e = \chi_i = 8m^2/s$ substitution. In these simulations the plasma current is ramped up to 15MA in 100 s (FIG. 9). An ohmic case and an ECRH case are presented (in the latter case, 20MW of ECRH are added at mid-radius from t = 30s onwards). The plasma Last Closed Flux Surface (LCFS) is prescribed to a constant D-shape throughout the simulation. Figures 10 and 11 display the dynamics of the internal inductance, the q-profile at the end of the ramp (t = 100 s) and the electron temperature profile at the middle of the ramp (t = 50 s) for the various transport models. Though significant differences between models appear on the electron temperature prediction (in particular inside the ECRH deposition in the ECRH case), the final q-profiles reached at the end of the ramp are rather close (for a given heating scheme). The difference between models on the *li*(3) prediction is also small, of the same order as for the present experiments, i.e. +/- 0.1. Thus, even in an ITER case with strong and narrow heating source, all selected transport models behave rather similarly in terms of *li* dynamics and target q-profile, providing a prediction envelope which, for the experimental validation dataset was containing the experimental value. As expected, the addition of ECRH during the current ramp is delaying the current penetration due to the decrease of the plasma resistivity with increasing electron temperature, with respect to the ohmic case. The internal inductance is lower by typically 0.05 – 0.15, which is significant owing to the rather narrow *li* operating space of the ITER PF systems [12]. While the target q-profile at t = 100 s is monotonic and sawtoothing in the ohmic case (sawtoothing was not included in the simulations), it is just above 1 and slightly hollow in the ECRH case. Earlier during the current ramp, when Ip reaches 9 MA at t = 42 s, the q-profile is slightly reversed in the ECRH case with a local minimum around q = 2, i.e. close to the target q-profile expected for the ITER "steady-state" scenario. This target q-profile control capability (also available with other electron heating schemes such as LHCD [10]) will be useful in view of carrying out advanced scenarios ("hybrid" or "steady-state") on ITER, which may require starting the main heating phase without the q = 1 surface being in the plasma. These trends in the comparison between the ECRH and ohmic cases are obtained with all the transport models retained in our selection.

In the simulations above, none of the used empirical models accounts for Internal Transport Barrier (ITB) (the model GLF23 potentially takes ITBs into account but does not trigger one here). When using the CDBM model, which well reproduces a JT-60U reversed-shear discharge [13], ECCD applied at mid-radius during the ITER current ramp-up triggers an ITB, delaying further the current penetration inside mid-radius and yielding a strongly reversed target q-profile (Fig. 12).

Those projections are documented with sensitivity analysis. Indeed the absolute value of *li* and its dynamics depend on physical parameters that are given when analyzing present experiments but which have to be assumed in case of projection to ITER. These are: effective charge, initial conditions, boundary conditions for the transport equations, plasma shape and last but not least electron density. Figure 13 presents such a sensitivity analysis on *Te* boundary condition *Tea* and *Zeff* dynamics in the case of the ohmic ITER ramp-up introduced at the beginning of this section and using the scaling-based model with H_{98} = 0.4. The impact of the *Tea* variation is relatively small (less than 0.05 in *li* at the end of the *Ip* ramp-up), while using high *Zeff* at the beginning of the current ramp-up makes a quite strong difference in *li* during the early phase, which eventually disappears at the end of the ramp-up.

3. INTEGRATED SIMULATIONS OF ITER CURRENT RAMP-DOWN

Figure 14 illustrates two possible ITER fast current ramp-down scenarios, simulated by the Astra code [14], one with an H-L back transition (left), the other maintaining the plasma in H-mode with the use of higher heating power (right). The main challenge with the H-L back transition is the sudden drop of pressure (see β_P on the figure), which may cause a significant inward shift of the plasma and contact to the wall. Conversely the scenario of plasma termination in H-mode has no significant drop of β_P, but features a large increase of *li* at the end of the discharge which could cause vertical instability when I_P reaches 3MA.

The fact that the plasma energy content changes so rapidly after the H-L transition points to the importance of a self-consistent simulation of plasma equilibrium using free boundary equilibrium solvers, together with the core transport equations and PF systems controller. Figure 15 shows one example of such a simulation carried out with JETTO and CREATE-NL [15], which was applied to an extract from Scenario-2 plasma containing both L-H and H-L transitions. Although the presently adopted ITER shape control system can cope with both L-H and H-L transitions, the latter can push plasma onto the inner limiter when the plasma energy content exceeds level of W_{th}>350MJ. Successful self-consistent simulation of ITER current ramp-down scenario with DINA-CH coupled to the CRONOS Integrated Modelling code can be found in [16].

Together with the plasma current, the plasma density must also be ramped down without causing excessive divertor power load and while controlling divertor detachment. Using a simple model of edge/core fuelling control, TSC simulations of the ramp-down from ITER burning flat-top were performed on ITER 15MA/200s termination scenario. The TSC [17], comprised of two-dimensional free boundary plasma equilibria and one-dimensional transport model (CDBM), describes time-evolution of the plasma shape and profile dynamics of the plasma current Ip and temperature as well as density. The plasma density was controlled by feedback on neutral gas puff from the edge and core fuelling like pellet injection. Two ramp-down scenarios have been studied, one keeping the edge/core fuelling control invariant ($f_{edge/core}$ = 0.8, Figure 16 left), in the other $f_{edge/core}$ is ramped down linearly from 0.8 at 500 sec to 0.0 (totally core fuelling) at t = 600s (Figure 16 right). Time-evolution of divertor neutral pressure p0 was solved by 0-dimensional model of particle flux from and to the plasma, accumulation and pumping-out dynamics of fuelling gas. The H-L mode transition was forced at 600s. Figure 16 shows the dynamics of some of the SOL/divertor parameters, which are quite different depending on the fuelling scenario. It thus follows that edge/core fuelling control during the termination of ITER discharge is a key operating instruction for a slow and safe density ramp-down from high-Q burning flat-top.

CONCLUSIONS

During the past two years, significant modelling efforts have been carried out throughout the world to simulate the current ramp up and ramp down phases of the 15 MA ITER reference scenario. In particular, a set of empirical heat transport models for L-mode (namely the Bohm-gyroBohm model and scaling based models with a specific fixed radial shape and $H_{96\text{-}L}$ = 0.6 or H_{IPB98} = 0.4) has been validated on existing experiments for predicting the *li* dynamics within +/- 0.15 accuracy during current ramp-up and ramp-down phases. Simulations using the Coppi-Tang or GLF23 models (applied up to the LCFS) overestimate or underestimate the internal inductance beyond this accuracy (more than +/- 0.2 discrepancy in some cases). The +/- 0.15 accuracy on *li* is obtained using the density profile peaking and the electron temperature boundary condition (at the LCFS) from the experiment, which of course is not possible for present extrapolations to ITER. Therefore the sensitivity of the predictions using these models has been quantified when applied to ITER current ramp-up simulations. Of course, the validity of extrapolating such empirical models from present devices to ITER can be questioned, precisely because they are empirical. The multi-machine approach adopted in the validation exercise (as well as in the scaling approach underlying some of the models) answers this partially. The difficulties of applying first principles based transport models such as GLF23 in the outer zone of the plasma $\rho > 0.8$ have been shown. This makes such models difficult to use in view of predicting the *li* dynamics.

Integrated modelling can now address operational aspects of the current ramp-up and ramp-down phases of ITER scenarios. This involves coupled free-boundary equilibrium solvers, core transport code and PF systems circuit equations including voltage controller, in order to test the capability of the ITER PF systems to handle the chosen scenario. The H-L back transition at the end of the burn is one of the challenging phases of the operation that must be prepared by such complex integrated simulations. Another challenging aspect is the modelling of the plasma breakdown, which sets the initial conditions prior to the current ramp-up. This should also be addressed in the future, likely with dedicated codes and models for describing the specific processes occurring during this phase (pre-ionization, burnthrough, …). Another key ingredient that should be integrated in the simulations is particle fuelling and transport, including core edge interaction in order i) to verify that the chosen scenario can be indeed fuelled and ii) to check the operational limits of the divertor. This work shows recent examples of such highly integrated simulations, which presently are far from routine usage. In the recent years, modelling codes have progressed technically to reach this high level of integration of the usual core transport equations with more and more operational aspects. Nonetheless, a strong effort of validation of the individual models used in these integrated simulations on existing experiments remains the backbone and starting point of any extrapolation procedure and a significant effort has still to be carried out in this area. Dedicated scaled experiments are interesting for this purpose [18]. Ultimately, the developed models and integrated simulators will provide an essential support to the preparation of ITER scenarios and operation.

ACKNOWLEDGEMENTS

This work was partly supported by EURATOM and carried out within the framework of the European Fusion Development Agreement. The views and opinions expressed herein do not necessarily reflect those of the European Commission. The views and opinions expressed herein do not necessarily reflect those of the ITER Organization.

REFERENCES

[1] Prail V., Belo P., Boerner P., Bonnin X. et al 2009 Nuclear Fusion **49** 075030

[2] Pereverzev G.V., Yushmanov P.N., Report IPP 5/98 (2002), Garching

[3] Artaud J.F., Basiuk V., Imbeaux F., Schneider M. et al 2010 Nuclear Fusion **50** 043001

[4] Cennacchi G. and Taroni A., Report JET-IR(88) 03

[5] Kaye S et al. 1997, Nuclear Fusion **37** 1303

[6] ITER Physics Basis 1999 Nuclear Fusion **39** 2137

[7] Erba M., Aniel T., Basiuk V. Becoulet A. and Litaudon X. 1998 Nuclear Fusion **38** 1013

[8] Jardin S.C. , Bell M.G. and Pomphrey N. 1993 Nuclear Fusion **33** 371

[9] Waltz R.E., Staebler G.M., Dorland W. 1997, Hammett G.W. et al, Physics of Plasmas **4** 2482

[10] Kim S., Artaud J.F., Basiuk V., Bécoulet A. et al 2009, Plasma Physics and Controlled Fusion **51** 065020

[11] Imbeaux F. and Peysson Y. 2005 Plasma Physics and Controlled Fusion **47** 2041

[12] Kessel C.E., Campbell D., Gribov Y., Saibene G. et al 2009, Nuclear Fusion **49** 085034

[13] Takei N., Nakamura Y., et. al. 2007, Plasma Physics and Controlled Fusion **49** 335

[14] Leonov M. et al 2010, 37th EPS Conf. on Plasma Physics and Controlled Fusion (Dublin, Ireland) P-2.182

[15] Albanese R., Mattei M., Calabrò G., Villone F., "Unified Treatment of Forward and Inverse Problems in the Numerical Simulation of Tokamak Plasmas", International Symposium on Applied Electromagnetics and Mechanics ISEM 2003, Versailles, France

[16] Kim S.H., Artaud J.F., Basiuk V., Dokuka V. et al 2009 Plasma Physics and Controlled Fusion **51** 105007

[17] Kessel C.E. et al 2007 Nuclear Fusion **47** 1274

[18] Jackson G.L., Politzer P.A., Humphreys D.A., Casper T.A. et al 2010 Physics of Plasmas **17** 056116

Parameter change	**Qualitative consequences**	**Impact on li**
Increase Te,edge by a factor 3	Lower resistivity, current diffuses slower	−0.05
Increase Zeff by 30 %	Higher resistivity, current diffuses faster	+ 0.06
Increase Ti,edge by a factor 2	Reduces electron to ion collisional heat exchange → increases Te	−0.02

Table 1 : Analysis of the impact of parameter uncertainties on the li prediction, from simulations of JET Pulse No: 71827 (ohmic) with the Bohm/gyro-Bohm model. The impact on li is the average change in internal inductance obtained at a given time slice, during the current ramp.

	Exp.	BgB	GLF23 ($\rho < 0.8$)	Scaling H98 = 0.4	Scaling H97 = 0.6
T(q = 1) (s)	2.4	3.1	2.7	2.3	2.3

Table 2: Tore Supra Pulse No: 40676. Time of occurrence of the first sawtooth in experiment (2st column) and of occurrence of the q = 1 surface in the simulations with various models.

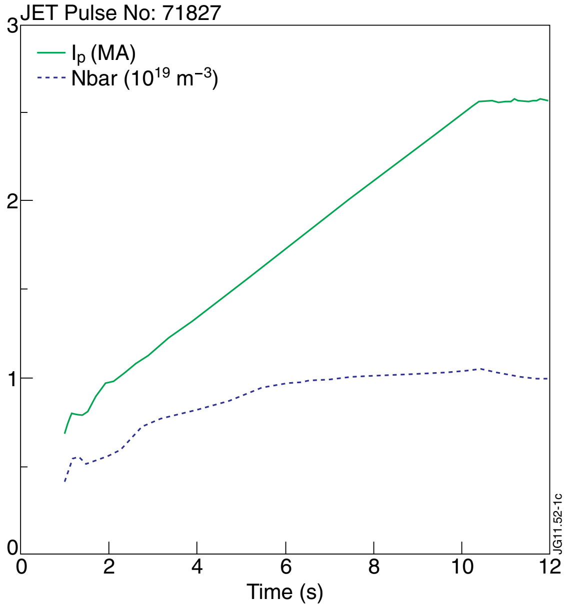

Figure 1 : Scenario of JET shot 71827 (ohmic). Time traces of plasma current Ip (green, solid) and central line averaged density Nbar (blue dots).

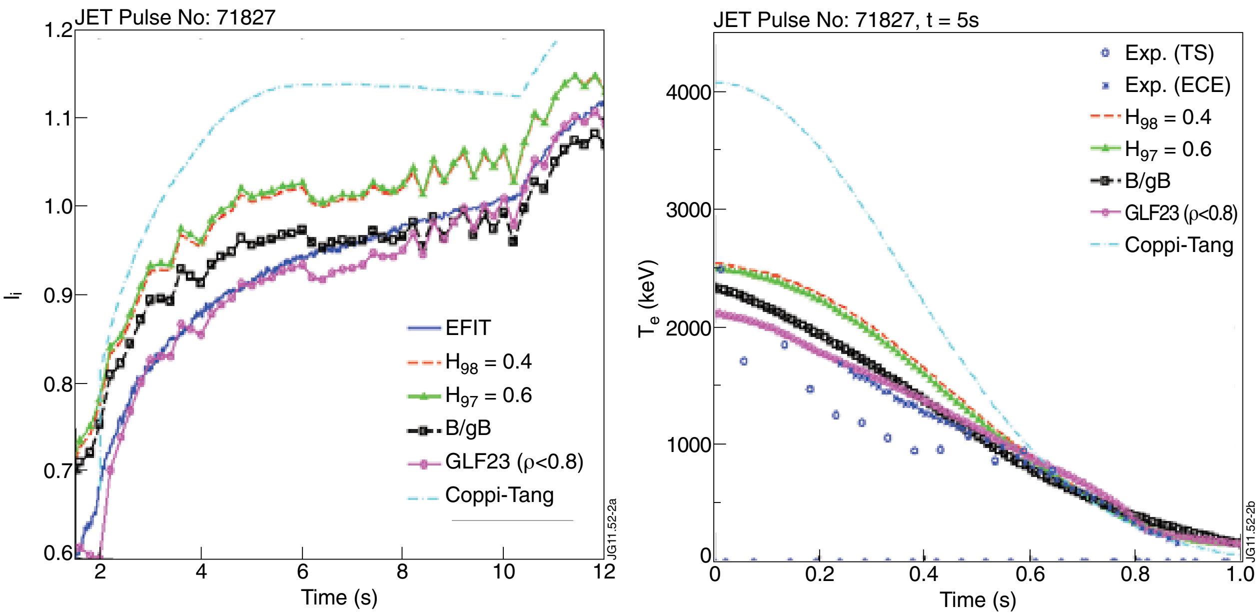

Figure 2 : Left : Simulation of the internal inductance dynamics of the JET ohmic shot 71827 with several heat transport models. The plasma current is ramped up to 2.5MA in 10s. Experimental value (EFIT reconstruction, blue), scaling-based (H_{98} = 0.4, red dash), scaling-based (H_L = 0.6, green triangles), Bohm/gyro-Bohm (black squares), GLF23 (applied only inside ρ = 0.8 with $\chi_e = \chi_i = 8\ m^2/s$ outside, purple), Coppi-Tang (light blue dash dotted). Right : Electron temperature profile at t = 5s. Blue circles and crosses indicate experimental measurements (Thomson Scattering and Electron Cyclotron Emission respectively), the other profiles correspond to the models predictions, same colour code as at left.

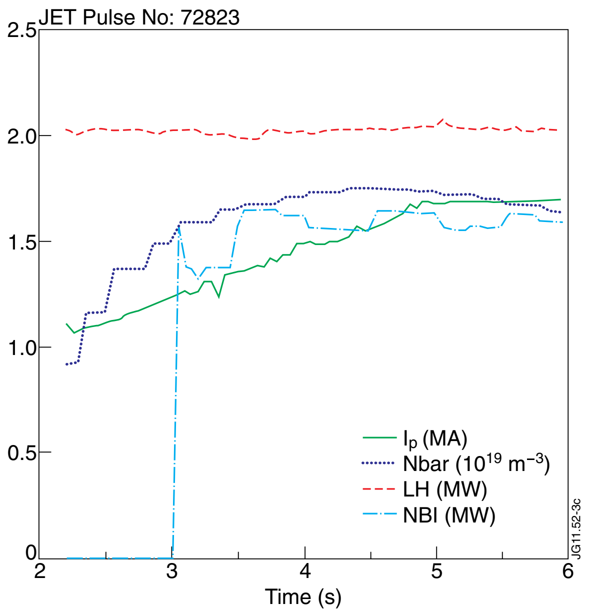

Figure 3: Scenario of JET Pulse No: 72823 (LHCD + NBI diagnostic beam). Time traces of plasma current I_P (green solid) central line averaged density Nbar (blue dots), LH power (red dash) and NBI (light blue dash dot).

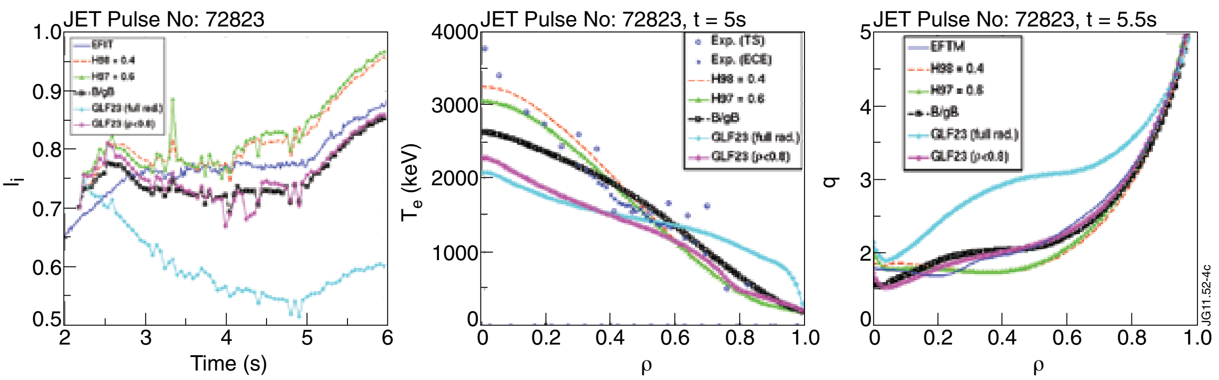

Figure 4 : Left : Simulation of the internal inductance dynamics of a JET LHCD assisted current ramp-up (2 MW of LHCD applied + 1.5MW NBI diagnostic beam) with several heat transport models. The plasma current is ramped up to 1.15MA in 5s. Same colour code as Fig.2. Middle : Electron temperature profile at t = 5s. Right : q-profile at t = 5.5s, with comparison to MSE constrained equilibrium reconstruction (blue, "EFTM").

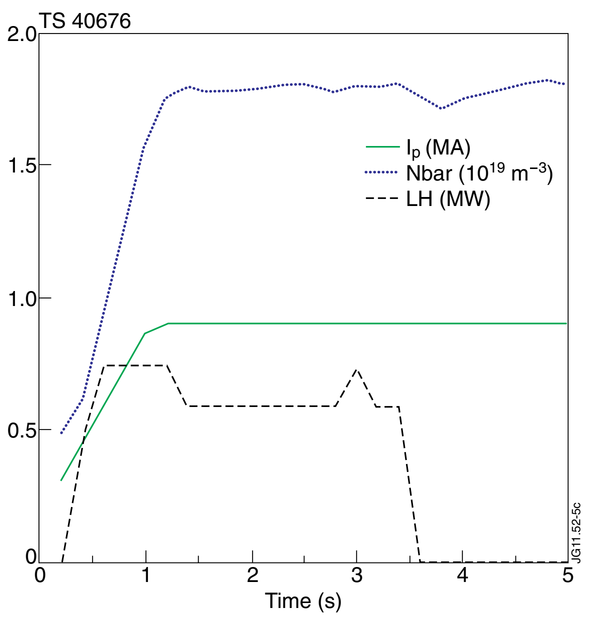

Figure 5 : Scenario of JET Pulse No: 72823 (LHCD + NBI diagnostic beam). Time traces of plasma current Ip (green, solid), central line averaged density Nbar (blue dots), ECCD power (black dash).

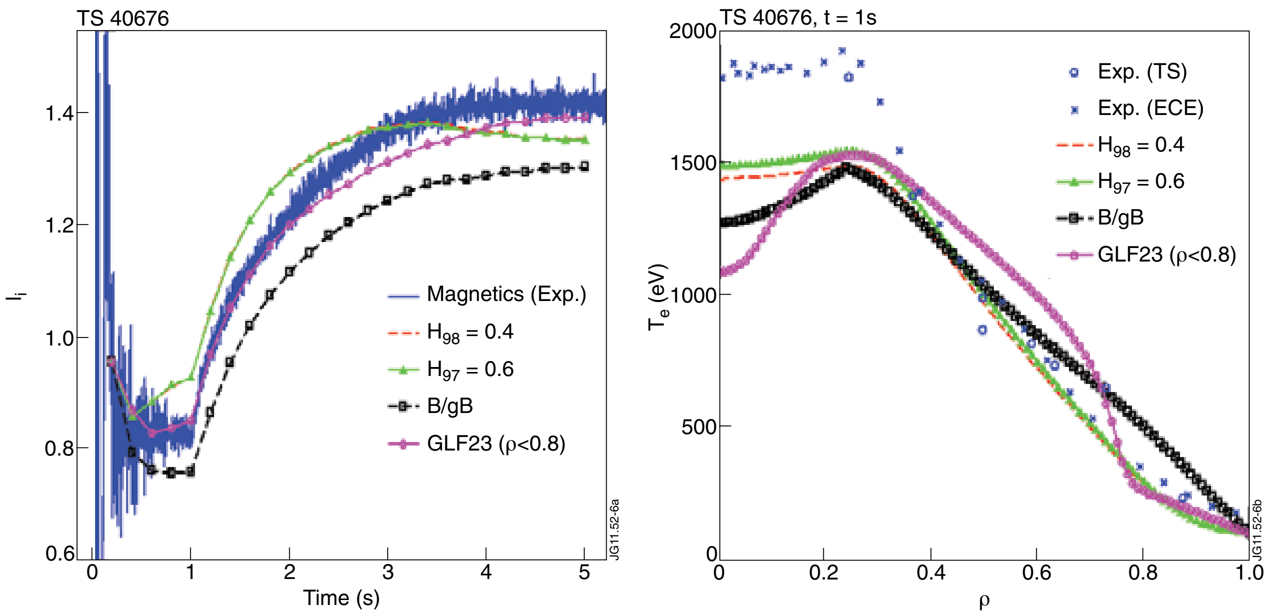

Figure 6 : Left : Simulation of the internal inductance dynamics of a Tore Supra ECCD assisted current ramp-up (co-ECCD applied at ρ = 0.3) with several heat transport models. The plasma current is ramped up to 0.9MA in 1s. Same colour code as Fig.2. Right : Electron temperature profile at t = 1s.

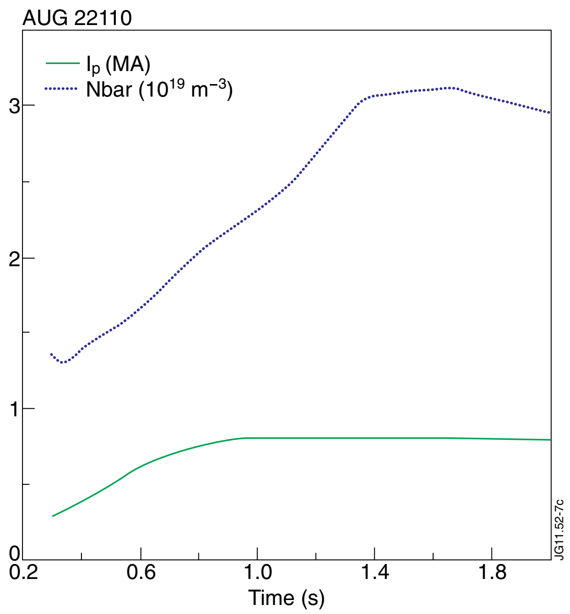

Figure 7 : Scenario of AUG shot 22110 (ohmic). Time traces of plasma current Ip (green, solid) and central line averaged density Nbar (blue dots).

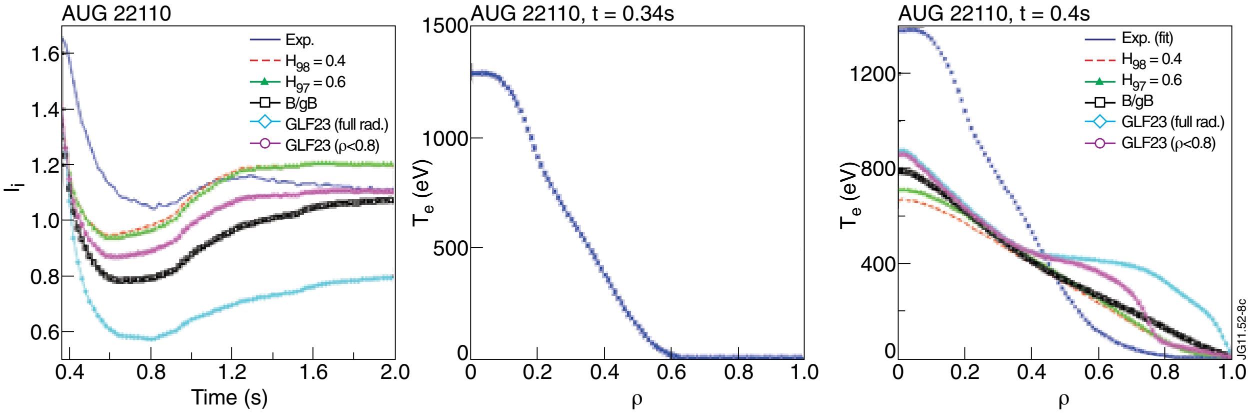

Figure 8 : Left : Simulation of the internal inductance dynamics of an AUG ohmic shot with several heat transport models. The plasma current is ramped up to 0.8MA in 0.9s. Same colour code as Fig.2. Middle : Electron temperature profile at t = 0.34s (fitted from measurements). Right : Electron temperature profile at t = 0.4s.

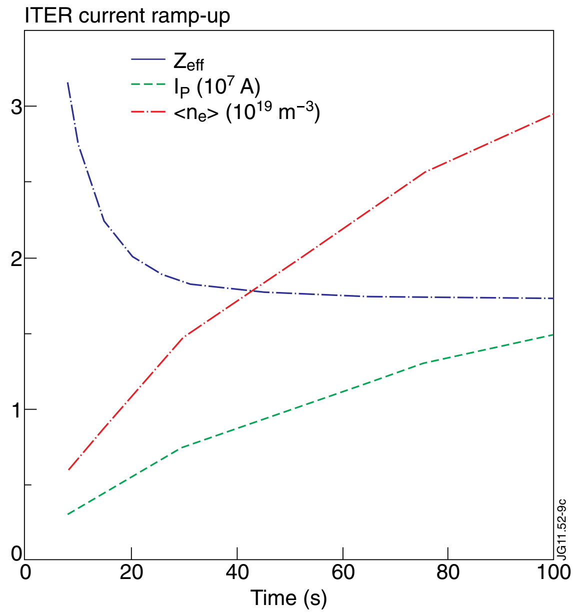

Figure 9 : Main reference time traces for the simulations of ITER current ramp-up. Effective charge Z_{eff} (blue, solid), plasma current (green, dash) and volume-averaged electron density (red, dash-dot). In the case with ECRH, 20MW ECRH are applied from t = 30s up to the end of the current ramp (t = 100s).

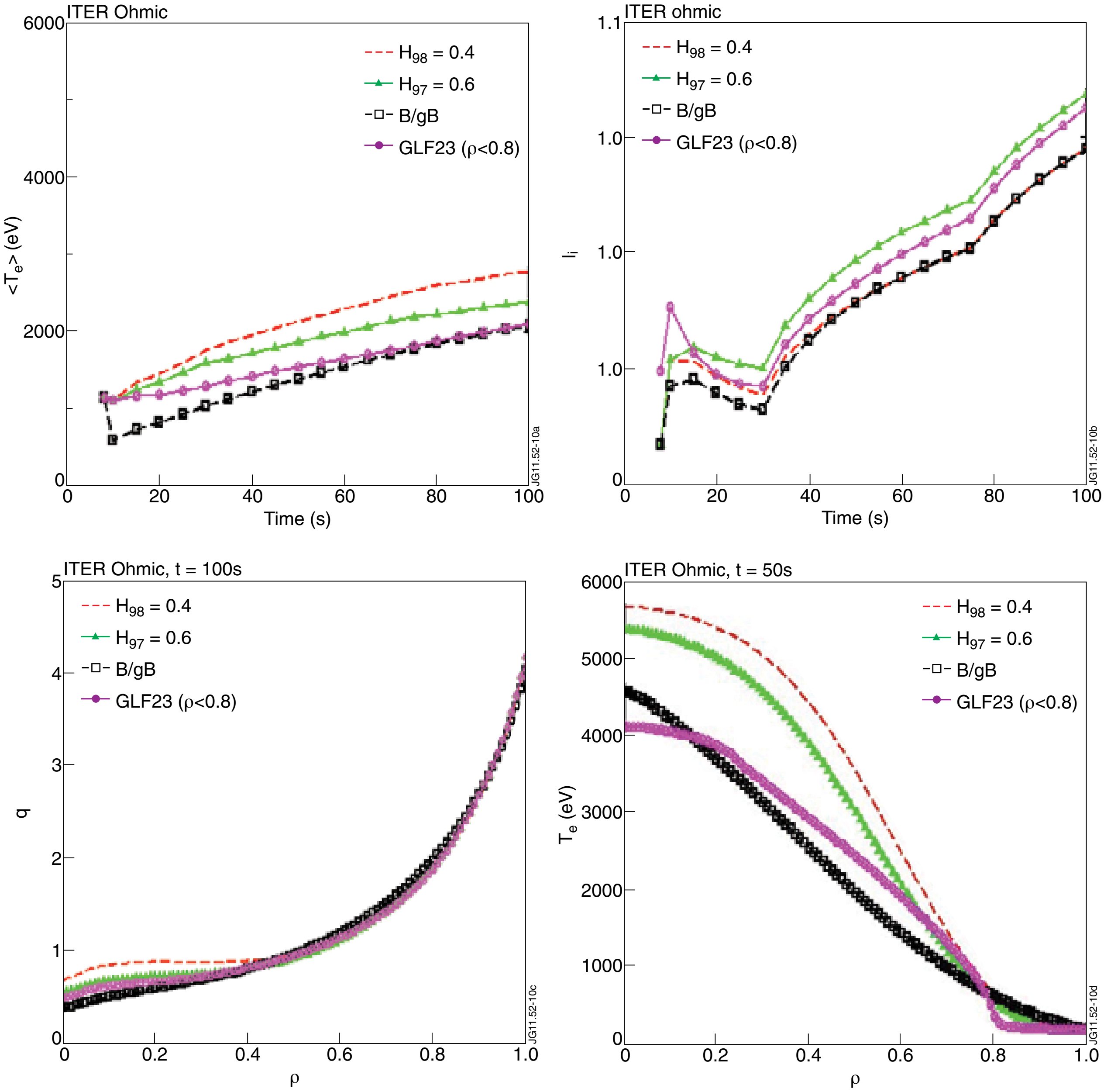

Figure 10 : Simulations of ITER current ramp-up in an ohmic case, using the following heat transport models: scaling-based (H_{98} = 0.4, red dash), scaling-based (H_L = 0.6, green triangles), Bohm/gyro-Bohm (black squares), GLF23 (applied only inside ρ = 0.8 with $\chi_e = \chi_i$ = 8m^2/s outside, purple). Top : time traces of the volume average electron temperature (left) and internal inductance (right). Bottom : q-profile at the end of the current ramp (left), electron temperature profile at the middle of the current ramp (right).

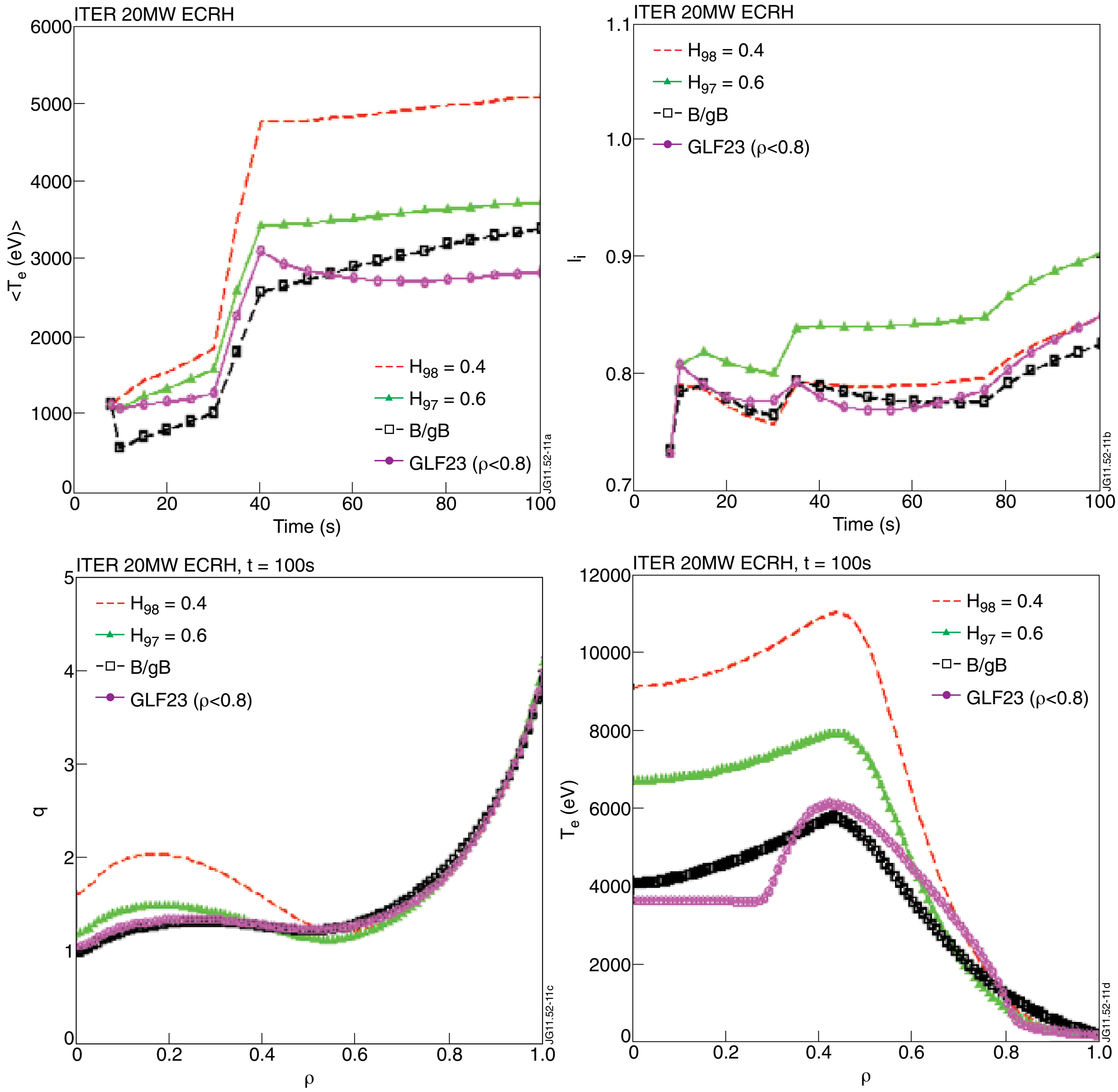

Figure 11 : Simulations of ITER current ramp-up in an ECRH case (20MW of ECRH are added at mid-radius from t = 30s onwards), using the same models and colour codes as in Figure 10. Top : time traces of the volume average electron temperature (left) and internal inductance (right). Bottom : q-profile at the end of the current ramp (left), electron temperature profile at the middle of the current ramp (right).

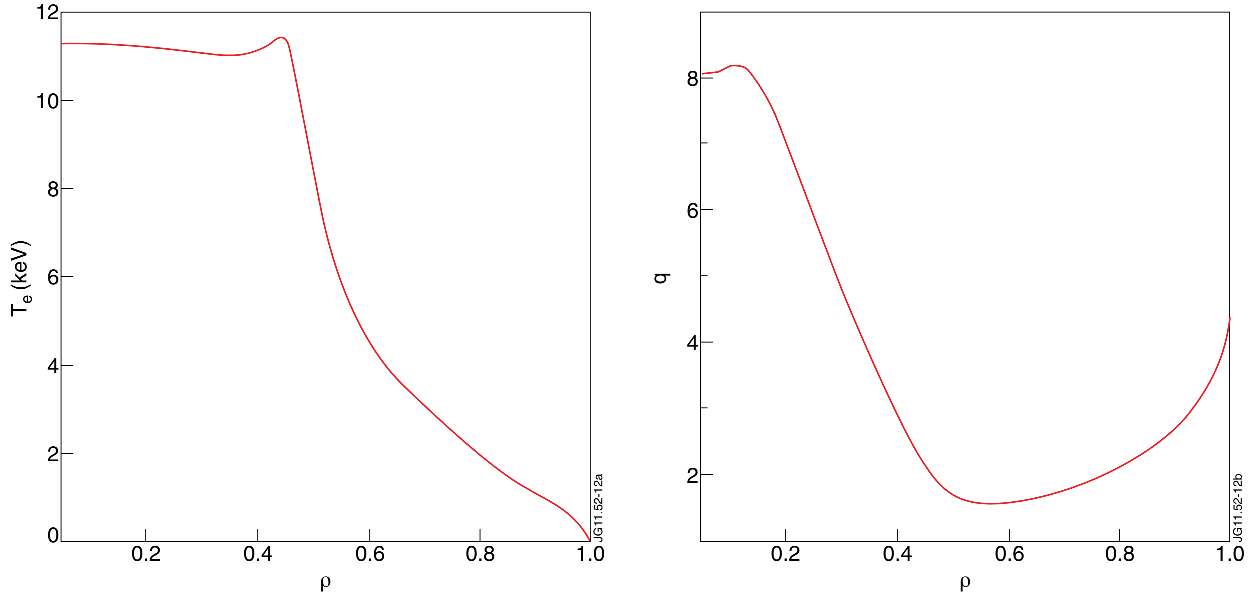

Figure 12: Projection of the ITER current ramp-up phase in case 20MW of ECRH are added at mid-radius early from t = 10s onwards (flat-top value I_p = 15MA reached at t = 70s). The dynamic evolution of plasma expansion is solved by the TSC code with the CDBM transport model. Electron temperature (left) and q-profile (right) at the end of the current ramp.

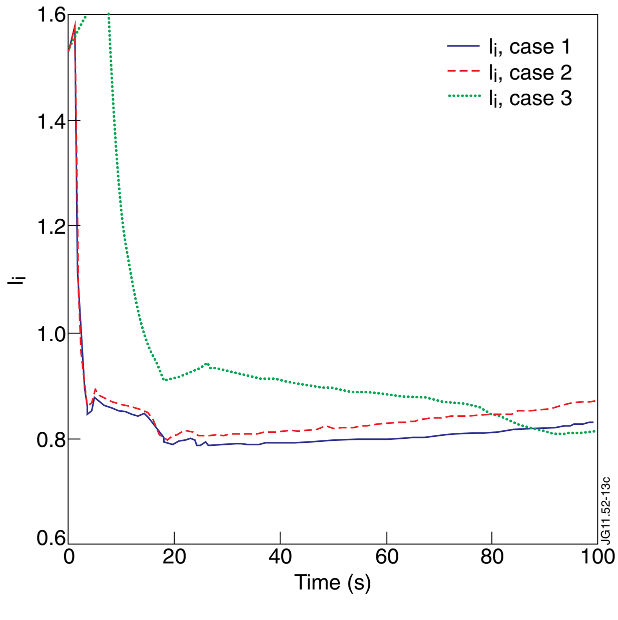

Figure 13: Sensitivity analysis in case of the ohmic ITER ramp-up case (flat-top value 15MA reached at t = 100s) with the scaling-based model H_{98} = 0.4. Case 1 (blue): constant Z_{eff} = 1.7, Tea ramped up from 25 to 250eV. Case 2 (red): constant Z_{eff} = 1.7, Tea 25-100eV. Case 3 (green): Z_{eff} ramped down from 4 to 1.7, Tea 25-250eV.

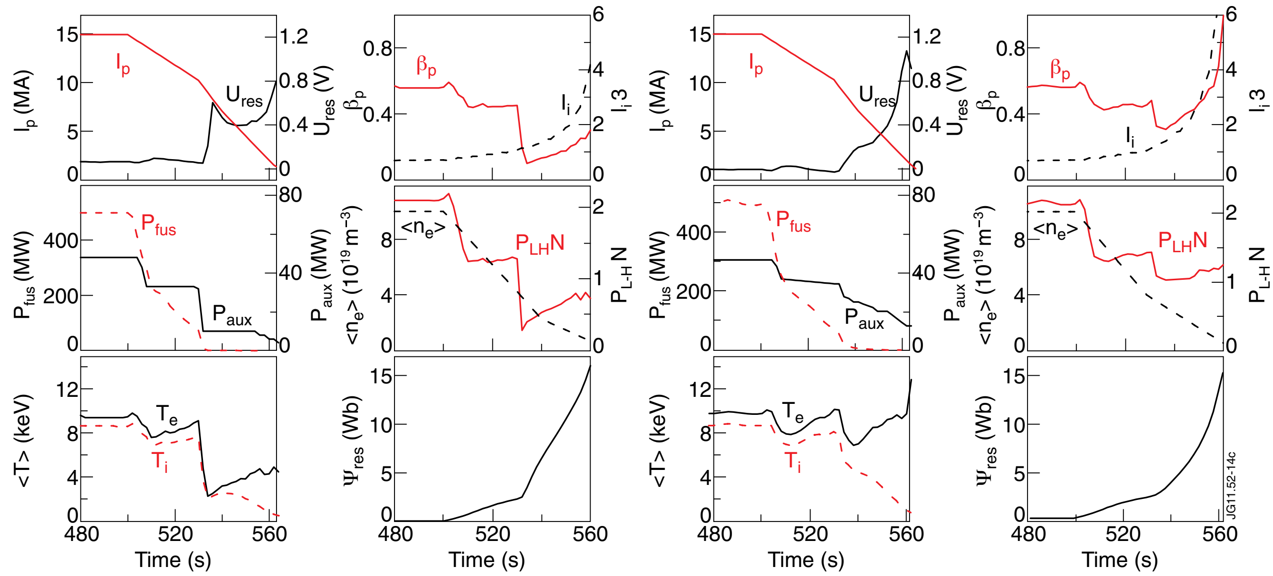

Figure 14: Plasma termination scenarios in L-mode (left, H-L transition triggered at t = 530s by decreasing the additional power Paux), and staying in H-mode (right), simulated with the Astra code.

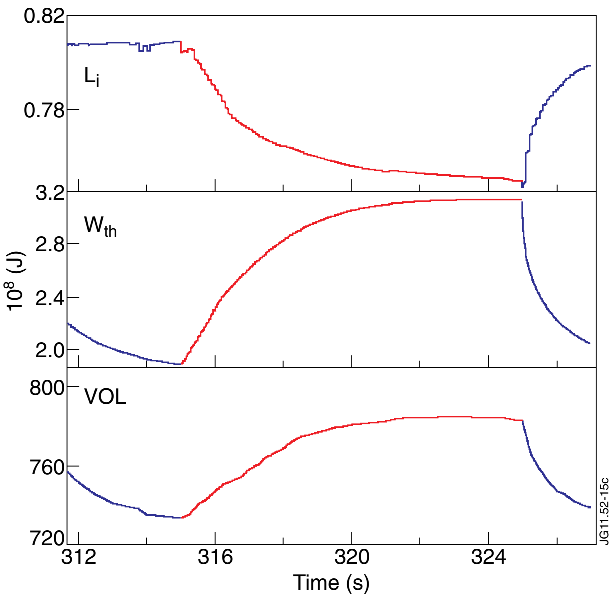

Figure 15. From top to bottom: internal inductance (plasma is in L-mode when colour is blue and in H-mode when colour is red), plasma thermal energy content and plasma volume

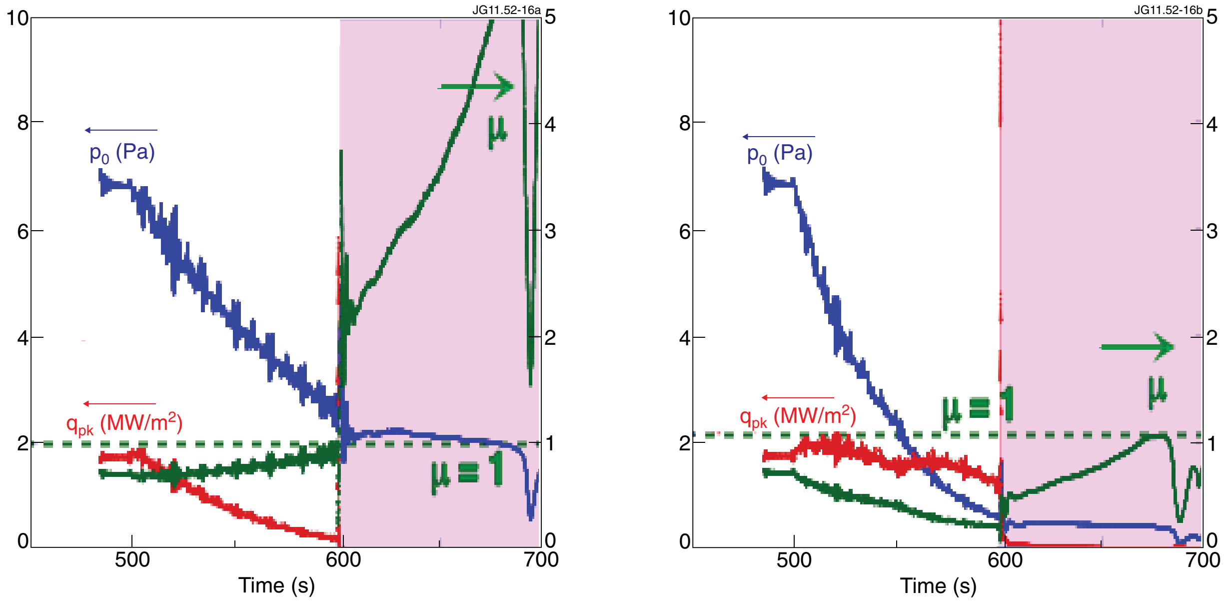

Figure 16: Left : Simulation of the divertor power load q_{pk}, the normalized neutral pressure μ and the divertor neutral pressure p_0, keeping the edge/core fuelling control invariant ($f_{edge/core}$ = 0.8). Right after H-L transition at 600sec, the operating point of inner divertor becomes strongly detached (μ >> 1). Right : Simulation of q_{pk}, μ and p_0, changing fedge/core from 0.8 at 500sec to 0 (totally core fuelling) at 600sec. Even after H-L transition, the operating point of inner divertor remains attached in "regime A" (μ < 1), though a higher heat pulse more than 10MW/m^2 arises at the H-L transition.